Numerical Investigation of the Aerodynamic Characteristics of a Streamlined Box Girder

Jianjun Zhang*

Guangzhou Salvage of the Ministry of Transport, Guangzhou, Guangdong, 510260, China

*Email: zhangjj@gzsalvage.cn

Abstract. A numerical investigation of the aerodynamic characteristics of a streamlined box girder was conducted based on computational fluid dynamics (CFD). The SST k–ω turbulence model was employed to simulate the flow field around the girder. The time histories of the three-component aerodynamic forces, the distribution of mean surface pressure, as well as the pressure and velocity contours of the flow field were systematically analyzed. The results reveal the flow behavior of the incoming air as it passes over the girder surface and elucidate the intrinsic relationship between flow characteristics and wind pressure distribution. The study provides a clearer understanding of the aerodynamic mechanisms governing the wind-resistant performance of streamlined box girders and offers a valuable reference for their aerodynamic design and optimization.

Keywords: Streamlined box girder; Computational fluid dynamics; Aerodynamic characteristics; turbulence model

1 Introduction

Streamlined box girders are widely used in modern long-span bridges because their optimized geometry can effectively reduce aerodynamic drag and improve wind-resistant performance. With the continuous increase in bridge span and structural flexibility, wind-induced effects such as vortex-induced vibration (VIV), flutter, and buffeting remain major concerns in bridge design, especially under complex wind environments including mountainous terrain and coastal regions. Recent reviews have highlighted that non-uniform inflow and turbulence characteristics in exceptional terrain can significantly amplify unsteady aerodynamic loads on bridge decks[1]. Wind tunnel testing has traditionally been regarded as the most reliable approach for evaluating the aerodynamic behavior of bridge girders. However, experimental studies are often limited by Reynolds number effects, model simplifications, and high testing costs, motivating the increasing use of computational fluid dynamics (CFD) as a complementary or alternative tool. Advances in numerical wind engineering have demonstrated that CFD can provide detailed information on aerodynamic forces, surface pressure distributions, and wake flow structures that are difficult to capture experimentally[2]

J. Zhang et al. (eds.), *Proceedings of the 2026 2nd International Conference on Engineering Management and Safety Engineering (EMSE 2026)*, Advances in Engineering Research 300,
https://doi.org/10.2991/978-94-6239-703-3_6

Among various turbulence modeling approaches, the SST k–ω model has been shown to perform well in predicting separated flows and near-wall behavior for bridge deck sections. Its applicability to streamlined box girders has been validated through comparisons with wind tunnel tests and full-scale measurements[3-4]. Recent CFD studies have further employed the SST k–ω model to investigate unsteady aerodynamic forces and vortex shedding characteristics of box-girder-type decks[5]. Vortex-induced vibration remains a critical issue for streamlined box girders, as lock-in phenomena can cause persistent oscillations and fatigue damage. CFD-based forced-vibration simulations have been successfully used to extract aerodynamic damping and predict VIV responses[6]. More recent numerical investigations have focused on the influence of auxiliary components and mitigation measures on pressure distribution and flow structures[7-8]. High-fidelity simulations, such as large-eddy simulation (LES), have also been applied to reveal three-dimensional wake characteristics of twin-box and streamlined girders[9].

Based on the above background, the present study conducts a CFD-based numerical investigation of the aerodynamic characteristics of a streamlined box girder using the SST k–ω turbulence model, aiming to clarify the internal relationship between flow features, surface pressure distribution, and wind-resistant performance.

2 Numerical Simulation Model

2.1 Model Configuration

The streamlined box girder prototype adopted for the present investigation is geometrically replicated as a scaled physical model, the detailed configuration of which is illustrated in Figure 1. In order to rigorously verify the numerical simulation accuracy and effectively eliminate the adverse influences induced by Reynolds number discrepancies between the numerical and experimental studies, the numerical model established herein is designed to be geometrically consistent with the experimental model, both following a unified scale ratio of 1:80. Based on this proportional scaling, the cross-sectional dimensions of the scaled box girder model are determined as follows: the overall width (B) is set to 387.5 mm and the vertical height (D) is fixed at 50 mm. Moreover, to ensure the precise reproduction of the actual aerodynamic profile of the prototype box girder and avoid the distortion of flow field characteristics caused by the simplification of structural details, the guardrail structures on both lateral sides of the main girder are completely preserved and meticulously modeled in the numerical setup without any geometric simplification. For comprehensive geometric parameters and dimensional details of the box girder cross-section, refer to the detailed illustration presented in Figure 1.

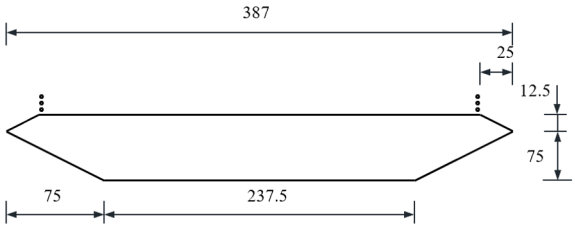

Fig. 1. Model configuration (unit: mm).

2.2 Numerical Methodology

The computational domain illustrated in Figure 2 extends 60B in the transverse direction and 30B in the vertical direction, resulting in a blockage ratio of approximately 0.25%, which is sufficiently small to minimize confinement effects. To enhance mesh quality and accommodate structural motion, the flow field is subdivided into three subdomains: a rigid region, a deformable region, and a stationary region. The rigid region employs body-fitted quadrilateral meshes with an initial wall-normal spacing of 1×10^{-5} m, which move synchronously with the structure to accurately resolve near-wall flow features, including flow separation, reattachment, and vortex shedding. The deformable region enables mesh deformation associated with structural vibration through dynamic meshing techniques, while the stationary region consists of fixed structured grids defining the outer boundaries of the computational domain. The lateral and vertical extents of the stationary region are sufficiently large to suppress boundary interference.

A hybrid meshing strategy is adopted, combining structured quadrilateral elements in the vicinity of the girder with unstructured quadrilateral elements in the transition zones, as shown in Figure 3. Boundary conditions are specified as no-slip walls on the girder surfaces, a uniform velocity inlet at the upstream boundary, a pressure outlet at the downstream boundary, and symmetry conditions at the upper and lower boundaries. The numerical simulations are conducted using the finite volume method implemented in ANSYS Fluent, with turbulence modeled by the SST k–ω model.

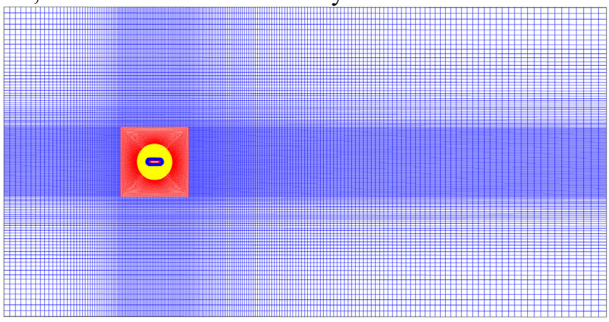

Fig. 2. The global view of the mesh

3 Results and Analyses

3.1 Mean Pressure Distribution

Figure 3 presents the longitudinal distribution of the pressure coefficient $\overline{C}_{pi}$ along the upper and lower surfaces of the structure, plotted as a function of the normalized streamwise coordinate X/B.

For the upper surface (Figure 3(a)), the pressure coefficient exhibits a pronounced negative peak near the upstream edge ($X/B \approx -0.4$), indicating a strong local suction associated with flow acceleration and separation effects at the leading corner. Downstream of this region, $\overline{C}_{pi}$ gradually recovers and approaches a nearly constant value over the mid-span section ($-0.2 \leq X/B \leq 0.3$), suggesting a relatively stable pressure distribution. A slight pressure variation is observed close to the downstream edge, which can be attributed to wake interaction and flow reattachment phenomena.

For the lower surface (Figure 3(b)), a similar trend is observed; however, the magnitude of the negative pressure peak is significantly larger, with the minimum value occurring around $X/B \approx -0.3$. This indicates stronger flow acceleration and pressure reduction on the lower surface in the upstream region. The pressure coefficient then increases steadily downstream, reaching a quasi-uniform distribution over the central portion of the surface. Minor fluctuations near the trailing edge suggest the influence of three-dimensional flow effects and vortex shedding.

Overall, the comparison between the upper and lower surfaces reveals clear asymmetry in pressure distribution, particularly in the upstream region, highlighting the combined effects of geometry and flow separation on the aerodynamic loading characteristics.

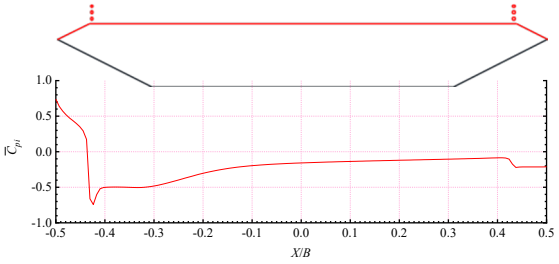

(a) Upper surface

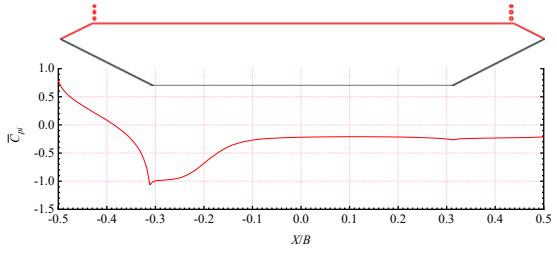

(b) Lower surface

Fig. 3. The mean value of wind pressure coefficient

3.2 Fluctuating Pressure Distribution

Figurre 4 depict the spanwise (X/B) evolution of the fluctuating pressure coefficient $\widetilde{C}_{pi}$ over the structural surface. Pronounced peaks in $\widetilde{C}_{pi}$ are evident at both spanwise extremities (X/B ≈ ±0.5), a phenomenon directly tied to the intense shear events associated with flow separation and reattachment at the structural edges, which drive vigorous pressure fluctuations. Within the mid-span platform region ($X/B \in [-0.4,0.4]$), the pressure fluctuations exhibit a more subdued, oscillatory profile.

Specifically, near the leading edge ($X/B \approx -0.5$), $\widetilde{C}_{pi}$ rises sharply to its maximum value, followed by a rapid decay between $X/B \approx -0.4$ and -0.3, corresponding to the transitional phase of the separated flow as it propagates onto the platform section. A distinct local elevation in $\widetilde{C}_{pi}$ occurs between X/B ≈ −0.2 and 0, indicative of the interplay between flow reattachment and secondary vortex structures in this zone. $\widetilde{C}_{pi}$ then declines and stabilizes from X/B ≈ 0 to 0.2, before forming a second peak at the trailing edge ($X/B \approx 0.5$) due to flow separation.

While the overall fluctuating pressure distribution patterns are consistent between the two datasets, the lower curve exhibits a systematically reduced $\widetilde{C}_{pi}$ amplitude. Furthermore, a flow feature is annotated near $X/B \approx -0.3$, highlighting a direct coupling between the pressure fluctuations in this region and the underlying shear-layer flow structures. This discrepancy underscores substantial variations in the energy distribution of surface pressure fluctuations under differing inflow conditions, offering critical experimental insights to advance the understanding of flow-structure interaction mechanisms.

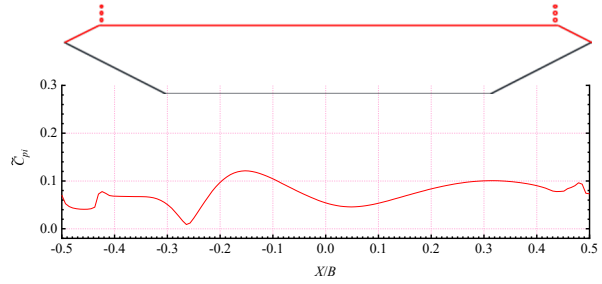

(a) Upper surface

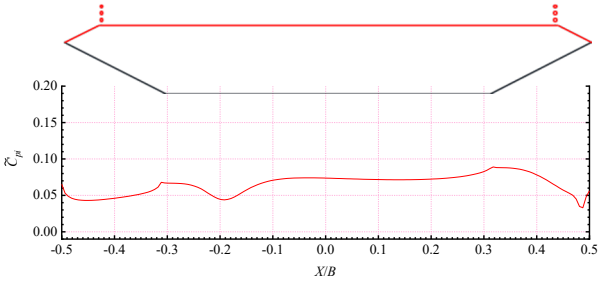

(b) Lower surface

Fig. 4. The standard deviation of wind pressure coefficient

3.3 Flow Field Characteristics

As shown in Figure 5 (a), a pronounced high-pressure region is formed at the upstream tip of the structure due to flow stagnation, with the maximum pressure occurring at the leading corner. Immediately downstream of this region, strong negative pressure zones develop along both the upper and lower surfaces, indicating rapid flow acceleration and local separation effects induced by the sharp geometry. The pressure gradually recovers along the midsection of the structure and approaches near-ambient levels in the far wake region. A relatively low-pressure wake is observed downstream of the trailing edge, reflecting the combined influence of flow separation and vortex shedding.

The velocity contours in Figure 5 (b) further clarify the flow characteristics. The incoming flow accelerates significantly along the upper and lower surfaces after passing the leading edge, forming high-velocity shear layers adjacent to the structure. A distinct low-velocity region appears in the near-wake downstream of the trailing edge, corresponding to flow separation and energy dissipation. The asymmetric velocity distribution near the leading edge suggests the presence of complex three-dimensional flow structures and strong velocity gradients, which are consistent with the pressure distribution observed in Figure 4(a).

Overall, the pressure and velocity fields demonstrate that the sharp-edged geometry induces strong flow acceleration, separation, and wake formation, which play a dominant role in determining the hydrodynamic (or aerodynamic) loading on the structure.

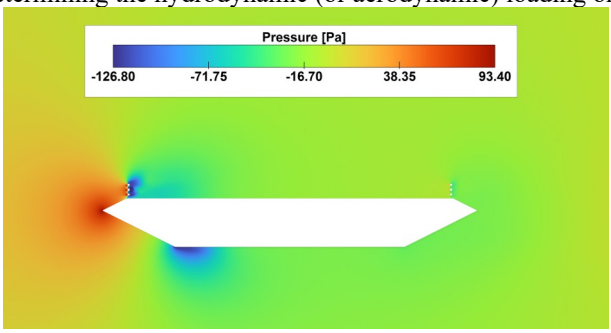

(a) Pressure contour

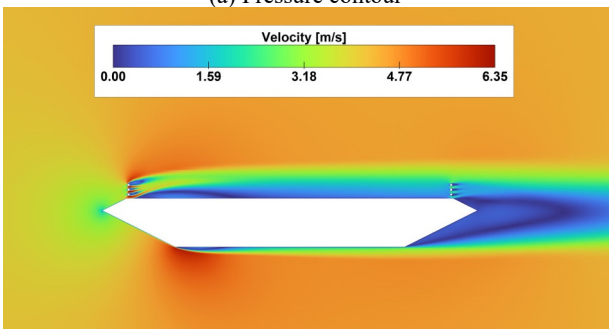

(b) Velocity contour

Fig. 5. Flow field Characteristics

4 Conclusion

A numerical simulation approach was employed to investigate the start-up performance of a streamlined box girder. The results indicate that various flow separation and reattachment phenomena occur as the airflow passes over the structural surface, leading to a distinct wind pressure distribution: positive pressure is observed only in the windward leading-edge fairing region, while negative pressure dominates the remaining surface areas. In addition, a negative pressure zone is formed in the wake region of the structure. Therefore, during aerodynamic configuration selection and design, targeted modifications to the start-up geometry can be implemented based on the wind pressure distribution to improve the overall start-up performance.

Reference

1. Li J, Yang S, Hao J, Gao G, Wang F, Bai H, Zhao G, Li Y, Xue X. Advances and applications of wind engineering in exceptional terrain. Journal of Traffic and Transportation Engineering (English Edition), 2024, 11(6): 1023–1209.
2. Zhang Y, MacReamoinn R, Cardiff P, Keenahan J. Analyzing wind effects on long-span bridges: A viable numerical modelling methodology using OpenFOAM for industrial applications. Infrastructures, 2023, 8(9): 130.
3. Kusano I, Cheynet E, Jakobsen J B, Snæbjörnsson J. Aerodynamic study of a suspension bridge deck by CFD simulations, wind tunnel tests and full-scale observations. IOP Conference Series: Materials Science and Engineering, 2021, 1201: 012007.
4. Daniotti N. Bridge Deck Aerodynamics: A Case Study in Full-Scale. Stavanger: UiS Scholarly Publishing Services, 2022.
5. Goktepeli I. Aerodynamic flow characteristics of a box girder and a twin-box girder: Comparison of k–ε and k–ω turbulence models. Journal of Engineering Science and Technology Review, 2024, 17(6): 73–83.
6. Wang Y, Chen X. Extraction of aerodynamic damping and prediction of vortex-induced vibration of bridge deck using CFD simulation of forced vibration. Journal of Wind Engineering and Industrial Aerodynamics, 2022, 224: 104982.
7. Wang X, Xu F, Zhang Z, Wang Y, Zhang M. Numerical explorations of the vortex-induced vibration of a streamlined box girder with water-filled barriers. Journal of Wind Engineering and Industrial Aerodynamics, 2023, 240: 105496.
8. Yao G, Zhang H, Li S, Chen Z. Investigation of vortex-induced vibration of bridge girders with aerodynamic mitigation measures. Journal of Marine Science and Engineering, 2023, 11(6): 1118.
9. Álvarez A J, Nieto F. Vortex-induced vibration analysis of a twin-box bridge deck by means of three-dimensional LES simulations. Journal of Wind Engineering and Industrial Aerodynamics, 2025, 258: 106015.